Two-sided Impacts of Warm Pool SSTs on Australian Precipitation Changes

Lei Fan,[1*] Sang-Ik Shin[2], Zhengyu Liu[3,4], and Qinyu Liu[1]

[1] Key Laboratory of Physical Oceanography / Collaborative Innovation Center of Marine Science and Technology, Ocean University of China, Qingdao, China.

[2] CIRES Climate Diagnostics Center, University of Colorado, and NOAA/Earth System Research Laboratory, Boulder, Colorado, USA

[3] Department of Atmospheric and Oceanic Sciences, University of Wisconsin-Madison, Madison, Wisconsin, USA

[4] Laboratory of Climate, Ocean and Atmospheric Studies, Peking University, Beijing, China.

* Correspondence to Lei Fan, E-mail: fanlei@ouc.edu.cn

This is the author manuscript accepted for publication and has undergone full peer review but has not been through the copyediting, typesetting, pagination and proofreading process, which may lead to differences between this version and the Version of Record. Please cite this article as doi: 10.1002/joc.4661

Abstract

Optimal tropical ocean regions for forcing precipitation changes over Australia are identified from maps of sensitivity of Australian precipitation to tropical sea surface temperature (SST) anomalies. These sensitivity maps are derived by a series of atmospheric general circulation model simulations with prescription of an array of SST anomaly patches over the tropics. The results show that the Australian precipitation changes are most sensitive to SST anomalies over the Indo-Pacific Warm Pool. There are competing opposing sensitivities such that warming over the Indian side of the Warm Pool increases precipitation, whereas that over the Pacific side decreases it. These sensitivity maps are validated by use in reconstruction of historical series of Australian precipitation with realistic interannual variability. The present results imply that monitoring and predicting the signs and magnitudes of SST anomalies over the critical Indo-Pacific Warm Pool may improve the prediction skills of Australian precipitation changes.

Keywords: Australian precipitation; sea surface temperature; sensitivity; Warm Pool

1 Background

The Australian continent is one of the driest inhabited landmass in the world and thereby drought-prone. The long-running droughts during the period from mid-1990s to late 2000s have plagued many areas of Australia, causing a major social-economic problem (Cai and Cowan, 2008; Ummenhofer *et al.*, 2009). The climate research community has been increasingly interested in understanding how Australian precipitation responds to climate change, to address the public concerns of regional water availability (Nicholls, 1989; Risbey *et al*., 2009; Ummenhofer *et al*., 2011; Cai *et al*., 2013).

In addition to influences of atmospheric internal variability such as the Southern Annular Mode (Hendon *et al.*, 2007), slow-varying sea surface temperature (SST) anomalies are also considered important in modulating and predicting Australian precipitation (Risbey *et al.*, 2009). During the warm (cold) phase of the El Niño-Sothern Oscillation (ENSO), for example, the Australian climate in late winter and spring (June through November) is much drier (wetter) than average, in response to the weakened (strengthened) Walker

circulation (McBride and Nicholls, 1983; Allan, 1988). The negative (positive) phase of Indian Ocean Dipole (IOD) mode (Ashok *et al*., 2003) increases (decreases) precipitation over southern and western Australia during austral winter and spring through atmospheric Rossby waves (Cai *et al*., 2011). In this line of reasoning, the long-running drought in southeastern Australia at the beginning of this century is attributed to an abnormally frequent occurrence of positive IOD events (Cai and Cowan, 2008; Ummenhofer *et al*., 2009). The warm phase of Indian Ocean Basin (IOB) mode has also been suggested to impact the Australian hydrologic cycle by inducing abnormal subsidence over northern Australia in late summer and early autumn which prolongs dry conditions during El Niño summers (Taschetto *et al*., 2011; Cai and van Rensch, 2013). Collectively, all these studies highlight the impacts of SST anomaly patterns represented by the first or second EOF mode (including ENSO, IOD, and IOB) on precipitation changes over certain regions of Australia in different seasons (Risbey *et al*, 2009).

However, these leading EOFs explain only 60% (45%) of SST variability in the tropical Pacific (Indian) Ocean, and may not be adequate to fully describe SST-forced precipitation changes (Timbal and Hendon, 2011; Smith and Timbal, 2012). For example, a strong El Niño event in 1997/1998 was associated with a moderate precipitation increase across most of Australia during spring, while a near-record high drought in the country was accompanied by only a modest El Niño event in 2002/2003. By comparing those two El Niño events, Wang and Hendon (2007) suggest that the fragile relationship

of ENSO-Australian precipitation is because precipitation changes in Australia are more sensitive to relatively weak SST anomalies at the eastern edge of the western Pacific Warm Pool, rather than those in the eastern tropical Pacific. Thus, it is pivotal to consider the impacts of SST anomalies over regions of strong sensitivity in diagnosing Australian precipitation changes, even though they are not directly associated with the well-recognized patterns of tropical SST variability such as ENSO, IOD, and IOB. Watterson (2010; 2012; 2013) performed simulations with SST anomalies prescribed over several key regions around the Australian continent, finding that warm SSTs east of Indonesia can reduce the simulated Australian rainfall, whereas those to the west can increase it. In Watterson (2010), the locations of those oceanic regions for the prescribed simulations was empirical and there were too few regions to cover the entire tropical basin. Therefore, it is unclear how important SSTs are over those regions compared with those over other tropical regions in the forcing of Australian rainfall. In other word, given a certain region of Australia, what is the sensitivity of its precipitation to SST anomalies over the entire tropical basin? Such comprehensive studies can facilitate a quantitative comparison and find the most influential SSTs in forcing Australian rainfall.

To address the above question, we analyzed a large ensemble of simulations in which an array of idealized SST anomalies over all tropical oceans was prescribed, and we quantitatively determined the sensitivity of Australian precipitation to tropical SST forcing. An atmospheric general circulation model (GCM) (see model introduction in

Section 2) was used. Ideally, one can estimate such sensitivity using fully coupled climate models that explicitly incorporate the impacts of air-sea interactions or observations. However, the current generation of fully coupled models has difficulty in simulating both means and variabilities of observed tropical SSTs (Shin and Sardeshmukh, 2011). Such shortfalls result in poor simulations of observed regional climate responses to tropical SST changes, and may affect the sensitivity measurements. Uncoupled atmospheric GCM simulations using observed SSTs are more successful in Australian monsoon simulations (Wang et al, 2005) than in Asian monsoon regions. Moreover, SST-forced climate responses of coupled and uncoupled simulations are essentially identical when coupled model-generated SSTs are used for uncoupled simulations (Chen and Schneider, 2014). We did not use statistical analyses of observations to measure the sensitivity in the present work, owing to the limited length of observed climate records. Such a constraint affects the sensitivity measures, especially over regions of weak SST variability, because of the relatively small signal-to-noise ratios (Shin *et al*, 2010); this signal-to-noise issue can be mitigated in modeling world by calculating ensemble means. In view of the above considerations, we used atmospheric GCM simulations.

The paper is organized as follows. We introduce the model, datasets, and method of sensitivity estimation in Section 2. In section 3, the sensitivity maps of Australian precipitation are derived and associated physical links between sensitivity patterns and

Australian precipitation are discussed. Finally, a summary and discussion are given in Section 4.

2 Model, data, and methods

The model used is Max Planck Institute for Meteorology (MPIM) ECHAM5 (Roeckner *et al.*, 2003) with resolution T42 (about 2.8°) in the horizontal and 19 levels in the vertical. In Perkins *et al*. (2007), ECHAM5 was suggested as one of the best models for simulating the statistics of Australian daily precipitation. Regarding interannual precipitation variability, to assess the realism of ECHAM5 simulations, we compared simulated historical series of annual precipitation rate anomalies with observations (Fig.1). The observational precipitation data were from Global Precipitation Climatology Project version 2 (Adler *et al.*, 2003) dataset. For the MPI-ECHAM5 simulations, we used 24 ensemble members, all forced by the same observed time-varying global SST (also known as GOGA (Global–Ocean–Global–Atmosphere), available from the International Research Institute for Climate and Society archive). However, these members all had different atmospheric initial conditions. Based on the peaks of Australian rainy seasons (Fig. 1a), we chose three regions of the country for the precipitation comparison. These are the northern (Fig.1b), southern (Fig.1c), and eastern Australia (Fig.1d) regions. Tropical northern Australia has a clear monsoon reversal between wet summers (northwesterly winds) and dry winters (southeasterly winds), while the southern extratropical Australia is characterized by dry summers and wet winters. In

between those two regions, we also selected eastern Australia as a separate target, because it is densely populated and has substantial precipitation variability, which is heavily influenced by external drivers such as El Niño (Risbey *et al*, 2009).

In Fig. 1b–d, solid and dashed lines respectively denote the ensemble mean and spread (represented by the standard deviation of 24 members). Over all three subdomains, simulated and observed time series show good correspondence, with correlation coefficients of 0.74 for northern (Fig. 1b), 0.73 for southern (Fig. 1c), and 0.60 for eastern Australia (Fig. 1d). These high correlations indicate that the MPIM-ECHAM5 can capture the essence of Australian precipitation interannual variability and its physical links with SST anomalies. Such strong correspondence between simulated and observed Australian precipitation demonstrates the accuracy of sensitivity results derived using the model.

Given the aforesaid confidence in using MPIM-ECHAM5 for the study of Australian precipitation, we performed a series of simulations to quantitatively determine the sensitivity of that precipitation to tropical SST forcing. In those simulations, an array of steady, localized SST anomaly patches in 43 tropical locations was superimposed on the climatological annual cycle of global SSTs. These patches were theoretically designed with geographical centers shown in Fig. 1a (red dots). All Indo-Pacific patches are of the same size, but the Atlantic ones are smaller to evaluate the narrow Atlantic basin. However, all patches had the same intensity of SST forcing, with a prescribed area-

average SST anomaly of 0.66°C. For each patch location, 20-member ensemble integrations of warm patches and 20 of cold were performed for 25 months (2 years), beginning in October.

Our patch experiments form a "fuzzy Green's function" of Australian precipitation response to tropical SST anomalies under the linear assumption (Barsugli and Sardeshmukh, 2002; Barsugli *et al*., 2006; Shin *et al*., 2010). The sensitivity value *S* was defined as atmospheric response to per unit forcing intensity of an SST anomaly, i.e., it measures the effectiveness of tropical SST in forcing Australian rainfall. If forcing intensity *F* is expressed as the product of SST anomaly *T* and its area ΔA, then the area-average precipitation response *P* to any tropical SST forcing can be expressed as $P = \boldsymbol{S}^{\mathrm{T}}\boldsymbol{F} + \varepsilon$. Here, $\boldsymbol{S}$ is a 43-component sensitivity vector with superscript "T" denoting transposition, $\boldsymbol{F}$ is a 43-component forcing vector representing the SST forcings, and ε is the error associated with linear approximation and the finite ensemble size of patch experiments. To determine a meaningful $\boldsymbol{S}$, we minimized ε by treating it as SST-independent Gaussian random noise. The following is a brief summary of how the sensitivity maps were obtained from the patch experiments.

Take the sensitivity of the *k*-th (*k*=1,2,…,43) patch for example. Based on the 40-member ensemble of patch experiments forced by the SST anomaly of the *k*-th patch, we can estimate raw precipitation sensitivity S_k to the *k*-th patch as

$S_k = P_k / F_k = P_k / \sum_j (T_{k,j} \cdot \Delta A_{k,j})$, where P_k is the area-average precipitation response to SST anomalies of the *k*-th patch. P_k is defined as half the difference between ensemble mean precipitation responses to warm and cold patch anomalies, $T_{k,j}$ denotes SST anomalies at the *j*-th model grid point of the *k*-th patch, and $\Delta A_{k,j}$ is the area element of that grid. The estimated 43 raw sensitivity values were then assigned to the geographic centers of corresponding patches to construct a noisy raw sensitivity map. Finally, we applied thin-plate smoothing spline procedures (Gu, 1989) based on the signal-to-noise ratio to minimize ε, thereby obtaining a more meaningful and smooth sensitivity map.

3 Results

3.1 Sensitivity maps

Figure 2 shows quantitative sensitivities of Australian precipitation to tropical SST anomalies over the three target regions defined in Fig. 1a, during their respective 3-month seasons of interest. These are sensitivity maps for northern Australia in DJF (Fig. 2a), eastern Australia in SON (Fig. 2b), and southern Australia in JJA (Fig. 2c). For the eastern Australia, we chose to show results of austral spring (SON) instead of its rainy season DJF to compare impacts of the IOD pattern and Eastern Pacific SSTs. A detailed discussion of seasonal dependence is in Section 3.2.

As aforementioned, the sensitivity values represent atmospheric responses to per-

intensity unit positive SST forcing (see Fig.2 caption for the definition of this unit). We see from Fig.2a-c that in general, Australian precipitation is most sensitive to SST anomalies over the Indo-Pacific Warm Pool. Interestingly, there are opposite sensitivities separated by nodal lines located around 130°E, such that the warming over the Indian side of Warm Pool increases precipitation, while that over the Pacific side decreases precipitation. Hence, our results clearly indicate that precipitation changes over Australia are largely controlled by the signs and relative magnitudes of SST anomalies over the eastern Indian and western tropical Pacific Oceans. For example, a uniform warming across the Indo-Pacific Warm Pool may have negligible impact on the precipitation changes because of cancelling effects from the two competing oceans. In contrast, any imbalances can cause abnormally wet or dry conditions over Australia.

If the sensitivity values have the dimension of temperature, then the sensitivity pattern can be viewed as a theoretically optimal forcing pattern for enhancing Australian rainfall. That is, among all possible SST anomaly patterns with the same root mean square (r.m.s.) amplitude, the one in line with the sensitivity map (i.e., a SST anomaly pattern with peaks over the western Pacific and eastern Indian Ocean) can maximize the precipitation response (Barsugli *et al.*, 2006). In this sense, any observed tropical SST anomaly patterns are considered possible subset realizations, but the sensitivity map is not necessarily one of those subset patterns. Over the Indian Ocean, the sensitivity pattern in spring (Fig. 2b) bears a likeness to the observed negative IOD pattern, so it is easy to

understand why a negative IOD has long been considered a key factor enhancing Australian rainfall (Ashok *et al.*, 2003; Cai *et al.*, 2008; Ummenhofer *et al*., 2009). The quantitative sensitivity analysis implies that the eastern Indian Ocean SST is more important in the IOD impacts on Australian precipitation variability.

Detailed patterns of sensitivity (Fig. 2a-c) indicate that the precipitation changes are to a lesser extent sensitive to SST anomalies in other tropical oceans. The eastern Pacific El Niño (La Nina) pattern does not appear in the sensitivity maps, but has previously been shown to be important to rainfall in Australia with dry conditions during El Niño events (McBride and Nicholls, 1983; Allan, 1988). To understand this discrepancy, we must keep in mind that our sensitivity value was defined as the precipitation response divided by a unit of forcing. Therefore, given the same precipitation response, regions with stronger SST forcing (amplitude of SST anomaly) tend to have smaller sensitivities. That is, regions such as the eastern Pacific do not necessarily have great sensitivity. Furthermore, when El Niño occurs, eastern Pacific SST anomalies are always concurrent with those over other regions. Hence it is the conjunction of all these SST anomalies that generates the Australian precipitation anomalies during El Niño. However, in our study the sensitivity values over the eastern Pacific were derived from simulations with SST prescription only over the eastern Pacific, so sensitivity values indicate only the influence of the eastern Pacific. Therefore, the patch experiment method provides a means to assess the relative importance of tropical SSTs in a model perspective. Although the El Niño

pattern is not highlighted in Fig.2, we still can see negative influences of the eastern Pacific, especially in DJF (Fig. 2a) when El Niño peaks. The present result theoretically implies that the El Niño pattern may not be the optimum one for forcing Australian Precipitation, although it certainly has a powerful influence because of its large SST magnitude. Regarding sensitivity over the tropical Atlantic Ocean, summer (DJF) precipitation in northern Australia is sensitive to warm Atlantic SST anomalies. This is in line with the other findings that the warming over the tropical Atlantic Ocean is positively correlated with precipitation changes over northern Australia (Lin and Li, 2012). In winter (JJA; Fig. 2c), however, sensitivity values over the tropical Atlantic Ocean have a sign opposite that in summer, indicating that general cooling over the tropical Atlantic can enhance precipitation over southern Australia.

In the foregoing, we analyzed the sensitivity of precipitation in the three target regions to tropical SSTs. One may speculate as to the accuracy of the sensitivity maps in Fig. 2. To examine robustness, we linearly reconstructed the three historical precipitation anomaly series using patterns of historical SST anomalies and those in Fig. 2a-c. We then compared this reconstructed precipitation with a standard series derived from the ensemble mean of "fully nonlinear" GOGA simulations using global SST prescription. We did this reconstruction by calculating the weighted sum of 43 prescribed anomalies. The *k*-th precipitation anomaly is the response to the *k*-th patch of the idealized SST anomaly, and the *k*-th weight is determined by projecting the observed SST anomaly

pattern on the *k*-th patch of the SST anomaly. The weighted sum is ultimately divided by an overlap factor associated with the superimposition of adjacent patches (Barsugli and Sardeshmukh, 2002).

Correlation coefficients between the reconstructed and standard series for the three cases are respectively 0.57 (Fig. 2d), 0.75 (Fig. 2e), and 0.72 (Fig. 2f). Long-term trends were also captured by the linear reconstruction. Such strong correspondence between the reconstruction and GOGA simulation indicates that precipitation responses to SST anomalies are basically linear, and that the sensitivity maps in our study are accurate and relevant. One may note that the simulated trends are different from observation (Smith, 2004; Murphy and Timbal, 2008; Berry *et al.*, 2011; Catto *et al.*, 2012). This discrepancy may be explained by the conclusions of Timbal and Hendon (2011) and Smith and Timbal (2012). They suggested that SST variability accounts for much of the interannual precipitation variability, but for the observed long-term trend of Australian precipitation, SST is not a main contributor. Thence, it is not surprising that the SST-only based GOGA simulations produced incorrect trends. This implies that the significance of our results lies more in interannual precipitation variability rather than low-frequency variability because of the limited capability of atmospheric GCMs.

3.2 Seasonal dependence

Given that the SST-forced precipitation changes depend upon both sensitivity and forcing, and that regions of strong sensitivity (e.g., Indian-Pacific Warm Pool in Fig. 2a-c) do not always coincide with those of strong SST forcing (e.g., eastern tropical Pacific in Fig. 1a), one may conjecture about the extent to which the historical SST anomalies affect Australian precipitation. In other words, which region has the greatest influence on that precipitation with consideration of its SST magnitude? Moreover, an overview of the seasonal variation of such sensitivity would be valuable. To address these issues, we re-estimated the sensitivities in Fig. 3 for the entire Australian mainland over the four seasons (shadings in the figure), and calculated the products of sensitivities and corresponding SST standard deviations (contours). Originally, we examined the four seasonal sensitivity maps for each sub-region of Australia as in Fig. 2. However, we found that the difference between sub-regions for a given season was much less than that between seasons for a given sub-region (figure not shown). Hence for simplicity, we just took all of Australia as our target; its seasonal sensitivity is portrayed in Fig. 3. We see that in general, the patterns of the product remain similar to the pattern of sensitivity except for a few minor contrasts, e.g., the impacts of SST anomalies near the date line are heightened by the relatively strong SST variability there. This gross similarity further emphasizes the critical importance of sensitivity rather than the forcing itself in regulating Australian precipitation change. Seasonally, the positive sensitivity area of the Indian Ocean expands from the southeastern Indian Ocean during DJF-MAM (Van and Cai, 2014) to most of that ocean during JJA-SON. Negative sensitivity over the west

equatorial Pacific has its largest magnitude in austral summer (DJF), and it weakens in winter (JJA). Over the eastern Pacific, a weak and nonuniform sensitivity pattern in all seasons implies that the eastern Pacific El Niño SST is not a theoretically optimal forcing of Australian rainfall. Tropical Atlantic Ocean SSTs, however, show a clear reversal of sensitivity values during DJF-MAM (positive) and JJA-SON (negative).

3.3 Physical links

We have analyzed the sensitivity maps of Australian precipitation to tropical SST anomalies. Overall, the Australian rainfall is most sensitive to the two-sided opposing SST anomalies over the Indian-western Pacific Warm Pool with slight seasonal differences. It is of interest how the SST anomaly patterns enhance Australian precipitation. To understand the dynamics connecting the SST pattern and changes to that precipitation, we reconstructed responses of precipitation, 850-hPa wind, and 200-hPa geopotential height to tropical SST anomalies with same patterns as the sensitivity maps but with a 1^{o}C r.m.s. amplitude across the basins of interest. These atmospheric responses are reconstructed as the weighted sum of responses to individual patches, and the weights are proportional to the integrated SST anomalies within their respective patches. Figure 4 shows such reconstruction of atmospheric responses to the optimal forcing pattern (with 1°C r.m.s. amplitude) shown in Fig. 2b for densley populated eastern Australia in austral spring (SON). To highlight the oppoing impacts of SST anomalies over the Indian Ocean and west-central tropical Pacific, we reconstructed separate responses to the forcing

pattern over the Indian Ocean-South China Sea (west of 130°E; Fig. 4a) and west-central tropical Pacific (130°E-160°W; Fig. 4b).

The warm SST anomalies over the eastern Indian Ocean induce Matsuno-Gill type baroclinic responses in the tropics (Fig. 4a) (Matsuno, 1966; Gill, 1980). A 200-hPa ridge is accompanied by low-level (850-hPa) wind convergence over the warm eastern Indian Ocean. In association with these tropical perturbations, atmospheric Rossby wave trains are excited and propagate into the extratropics, generating cyclonic circulations over southwestern Australia and anticyclonic ones across southeastern Australia. A surface equivalent barotropic response associated with such upper tropospheric Rossby wave propagation is the confluence of moisture-laden 850-hPa winds from the equatorial Indian Ocean and South Pacific (near New Zealand) over eastern Australia, which augments precipitation there.

A tropical circulation response to the cool west-central Pacific (Fig. 4b) is a Matsuno–Gill type baroclinic anomaly of equatorial heat-sinks, i.e., a 200-hPa trough is accompanied by low-level (850-hPa) wind divergence with a pair of equatorial Rossby waves indicated by the 850-hPa anticyclones over the western Pacific. It is the anticyclone anchored in the South Pacific near the date line that transports maritime moisture-laden air to northern and eastern Australia, which increases precipitation there.

4 Summary and discussion

We quantitatively determined the sensitivity of Australian precipitation to tropical SST anomalies and identified the key tropical ocean areas using a series of MPIM-ECHAM5 simulations. Our results indicate that Australian precipitation changes are very sensitive to opposing SST anomalies over the Indo-Pacific Warm Pool. Warming on the Indian side of the Warm Pool increases precipitation, whereas that over the Pacific side reduces it. Positive sensitivity over the eastern Indian Ocean is accompanied by a relatively weak opposing negative sensitivity to its west. On the western Pacific side, a negative sensitivity pattern multiplied by the actual SST standard deviation shows a maximum center near the dateline, suggesting that the conventional relationship between Australian drought and El Niño may be fragile unless the importance of Warm Pool El Niño events (Kug et al, 2009) is given greater attention. The accuracy and relevance of our sensitivity maps were validated by comparing a reconstructed historical precipitation anomaly series with that from GOGA ensemble means. Seasonal dependence of those maps was also addressed.

The eastern Indian Ocean and eastern Pacific have long been considered important in forcing Australian precipitation. However, insufficient importance has been attached to western-central Pacific SST because of its week SST variability. This study together with other recent ones (Watterson, 2012; Watterson, 2013) may draw more research attention to the Warm Pool SSTs. These investigations indicate that Australian precipitation depends on the signs and detailed patterns of SST anomalies over those critical ocean

areas because the Pacific and Indian sides of the Warm Pool have opposing sensitivities.

The present results have limitations. Australian rainfall variations were not fully linked to SSTs, especially for low-frequency precipitation trends (Timbal and Hendon, 2011; Cai *et al*., 2014). Thus the present results are confined to the interannual variability of Australian precipitation. Moreover, those results are limited by model skill because they are from a purely modeling study using only one model. Further studies using multiple models are expected to furnish greater understanding of Australian precipitation variability.

Acknowledgements

We thank the two anonymous reviewers for their comments on the manuscript. This work is supported by the Ministry of Science and Technology of China (National Basic Research Program of China 2012CB955603; 2012CB955200), the Strategic Priority Research Program of the Chinese Academy of Sciences (Grant No. XDA11010203), the Natural Science Foundation of China (Grant No. 41176006; 41221063; 41406001; 41476003), and the Fundamental Research Funds for the Central Universities (Grant No.

201413029; 201562030).

REFERENCES

Adler RF, Coauthors. 2003. The version-2 Global Precipitation Climatology Project (GPCP) monthly precipitation analysis (1979–present). *J. Hydrometeor*., **4**:1147–1167.

Allan RJ. 1988. El Niño southern oscillation influences in the Australian region. *Prog. Phys. Geogr*. **12**: 313–348.

Ashok K, Guan Z, Yamagata T. 2003. Influence of the Indian Ocean Dipole on the Australian winter rainfall. *Geophys. Res. Lett.*, **30**: 1821, doi:10.1029/2003GL017926.

Barsugli JJ, Sardeshmukh PD. 2002. Global atmospheric sensitivity to tropical SST anomalies throughout the Indo-Pacific basin. *J. Climate*, **15**: 3427–3442.

Barsugli, J. J., S-I. Shin, and P. D. Sardeshmukh, 2006. Sensitivity of global warming to the pattern of tropical ocean warming. *Climate Dyn.*, **27**: 483–492

Berry G, Reeder M J, Jakob C. 2011. Physical mechanisms regulating summer time rainfall over Northwestern Australia. *J. Climate*, 24: 3705-3717.

Cai W, Rensch P van. 2013. Austral summer teleconnections of Indo-Pacific variability: Their nonlinearity and impacts on Australian climate. *J. Climate* **26**: 2796–2810.

Cai W, Cowan T. 2008. Dynamics of late autumn rainfall reduction over southeastern Australia. *Geophys. Res. Lett*. **35**: L09708, doi:10.1029/2008GL033727.

Cai W, van Rensch P, Cowan T, Hendon TH. 2011. Teleconnection pathways of ENSO and the IOD and the mechanisms for impacts on Australian rainfall. *J. Climate* **24**: 3910–3923.

Cai W, Purich A, Cowan T, van Rensch P, and Evan Weller. 2014. Did Climate Change–Induced Rainfall Trends Contribute to the Australian Millennium Drought?. *J. Climate*, **27**, 3145–3168.

Catto J L, Jakob C, Nicholls N. 2012. The influence of changes in synoptic regimes on North Australian wet season rainfall trends, *J. Geophys. Res. Atmos.*, 117, doi: 10.1029/2012JD017472

Chen H, Schneider EK. 2014. Comparison of the SST-forced responses between coupled and uncoupled climate simulation. *J. Climate*, **27**: 740-756.

Gill AE. 1980. Some simple solutions for heat-induced tropical circulation. *Quart. J. Roy. Meteor. Soc.*, **106**: 447–462.

Hendon HH, Thompson D W J, Wheeler Matthew C, 2007. Australian Rainfall and Surface Temperature Variations Associated with the Southern Hemisphere Annular Mode. *J. Climate*, **20**: 2452–2467.

Kug J-S, Jin F-F, An S-I, 2009. Two types of El Niño events: cold tongue El Niño and warm pool El Niño. *J. Climate*, 22, 1499-1515. Doi: http://dx.doi.org/10.1175/2008JCLI2624.1

Lin Z, Li Y. 2012. Remote influence of the tropical Atlantic on the variability and trend in North West Australia summer rainfall. *J. Climate* **25**: 2408–2420.

Matsuno T. 1966. Quasi-geostrophic motions in equatorial areas. *J. Meteorol. Soc. Jpn*. **2**: 25-43.

McBride JL, Nicholls N. 1983. Seasonal relationships between Australian rainfall and the Southern Oscillation. *Mon. Wea. Rev*. **111**: 1998–2004.

Murphy BF and Timbal B. 2008, A review of recent climate variability and climate change in southeastern Australia. *Int. J. Climatol.*, 28: 859–879. doi: 10.1002/joc.1627

Nicholls N. 1989. Sea surface temperatures and Australian winter rainfall. *J. Climate*. **2**: 965–973.

Palmer, T. N. and D. A. Mansfield. 1984. Response of two atmospheric general

circulation models to sea-surface temperature anomalies in the tropical east and west Pacific. *Nature* **310**: 483–485.

Perkins SE, Pitman AJ, Holbrook NJ, Mcaneney J. 2007. Evaluation of the AR4 climate models' simulated daily maximum temperature, minimum temperature, and precipitation over Australia using probability density functions. *J. Climate*, **20:** 4356–4376.

Risbey JS, Pook MJ, McIntosh PC, Wheeler MC, Hendon HH. 2009. On the remote drivers of rainfall variability in Australia. *Mon. Wea. Rev*. **137**: 3233–3253.

Roeckner E, Collaborators. 2003. The atmospheric general circulation model ECHAM5. Part I: Model description. *Max Planck Institute for Meteorology Rep*. 349, 127 pp.

Shin SI, Sardeshmukh PD. 2011. Critical influence of the pattern of Tropical Ocean warming on remote climate trends**.** *Climate Dynamics* **36**(7-8): 1577-1591

Shin SI, Sardeshmukh PD, Pegion K. 2010. Realism of local and remote feedbacks on tropical sea surface temperatures in climate models, *J. Geophys. Res.*, **115**: doi:10.1029/2010JD013927.

Shin SI, Sardeshmukh PD, Webb RS. 2010. Optimal tropical sea surface temperature forcing of North American drought. *J. Climate* **23**: 3907–3917.

Smith I. 2004. An assessment of recent trends in Australian rainfall. *Australian meteorological Magazine*, 53: 163-173.

Smith IN, Timbal B. 2012. Links between tropical indices and southern Australian rainfall, *Int J. Climatol* 32: 33-40.

Taschetto AS, Gupta AS, Hendon HH, Ummenhofer CC, England MH. 2011. The contribution of Indian Ocean sea surface temperature anomalies on Australian summer rainfall during El Niño events. *J. Climate* **24**: 3734–3747.

Timbal B, Hendon H. 2011. The role of tropical modes of variability in recent rainfall deficits across the Murray-Darling Basin, *Water Resour. Res.*, **47**: W00G09, doi:10.1029/2010WR009834.

Ummenhofer CC, Collaborators. 2009. What causes Southeast Australia's worst droughts?

Geophys. Res. Lett. **36**: L04706, doi:10.1029/2008GL036801.

van Rensch, P. and W. Cai. 2014. Indo-Pacific–induced wave trains during austral autumn and their effect on Australian rainfall. *J. Climate* **27**: 3208–3221.

Wang B, Ding Q, Fu X, Kang IS, Jin K, Shukla J, Doblas-Reyes F. 2005. Fundamental challenge in simulation and prediction of summer monsoon rainfall. *Geophys. Res. Lett*. **32:** L15711, doi:10.1029/2005GL022734.

Wang G, Hendon H. 2007. Sensitivity of Australian rainfall to inter–El Niño variations. *J.* Climate **20**: 4211–4226.

Watterson I G. 2010. Relationships between southeastern Australian rainfall and sea surface temperatures examined using a climate model. *J. Geophys. Res.*, 115, D10108. doi:10.1029/2009JD012120

Watterson I G. 2012. Understanding and partitioning future climates for Australian regions from CMIP3 using ocean warming indices. *Climatic Change*, 111, 903-922, doi:10.1007/s10584-011-0166-x

Watterson I. G. 2013. Climate change simulated by full and mixed-layer ocean versions of CSIRO Mk3.5 and Mk3.0: the Asia-Pacific region. *Asia-Pacific J. Atmos. Sci*, **49**(3), 287-300, doi:10.1007/s13143-013-0028-8

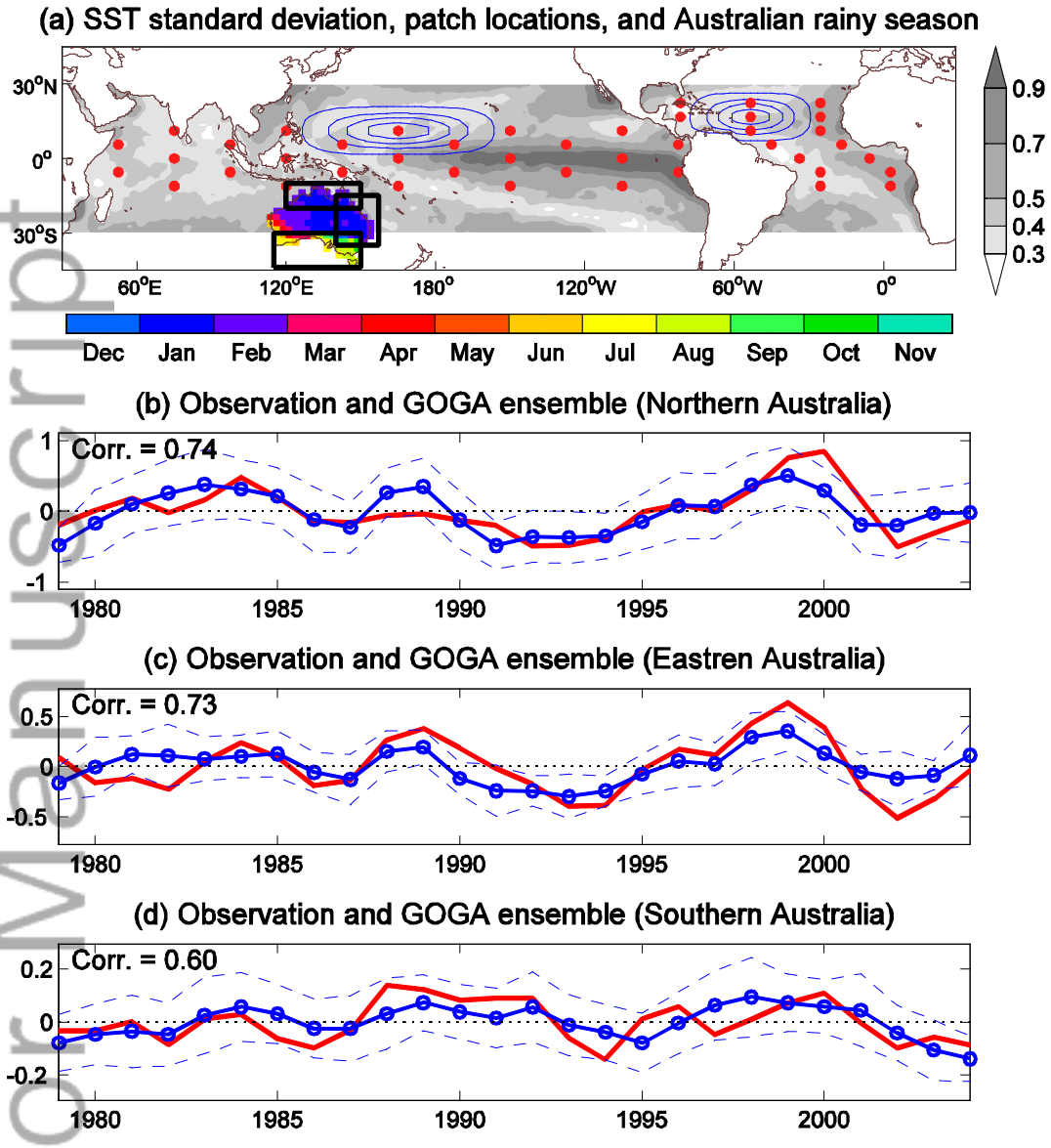

Fig. 1 (**a**) Patch locations and timing of Australian rainy season. Red dots denote geographic centers of each patch. Typical SST anomalies over the Indo-Pacific and Atlantic oceans are shown by blue contours from 0.1 to 1.6 °C with an interval of 0.5 °C. Gray shading depicts standard deviations of annual mean SSTs. The three target regions of the study are indicated by thick black rectangles in (a), and color shading in those rectangles indicate the rainy season peak by month. (**b**)–(**d**) Comparisons between observed (red solid curves) and GOGA-derived

annual precipitation rate anomaly (units: mm/day) for (b) northern, (c) eastern, and (d) southern Australia, respectively. Ensemble mean is shown by blue curves with open circles, and dashed blue lines indicate ensemble spread.

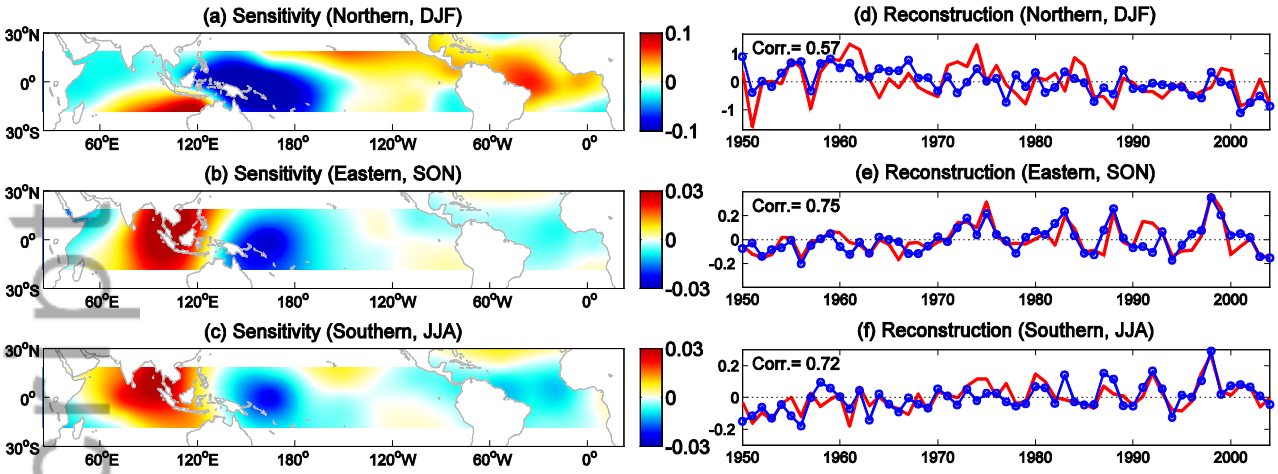

Fig. 2 Precipitation sensitivity maps for (**a**) northern Australia in DJF, (**b**) eastern Australia in SON, and (**c**) southern Australia in JJA. Sensitivity values represent precipitation responses (units: mm day^{-1}) to a uniform 1 °C SST warming over a large (10^6 km^2) ocean area centered at corresponding locations. (**d**), (**e**), and (**f**) portray linearly reconstructed time series (blue curves with open circles) of area-average precipitation anomalies in respective seasons, for comparison with standard time series (red curves) derived from GOGA ensemble means. Correlation coefficients between the two series are in the upper left corner of each panel..

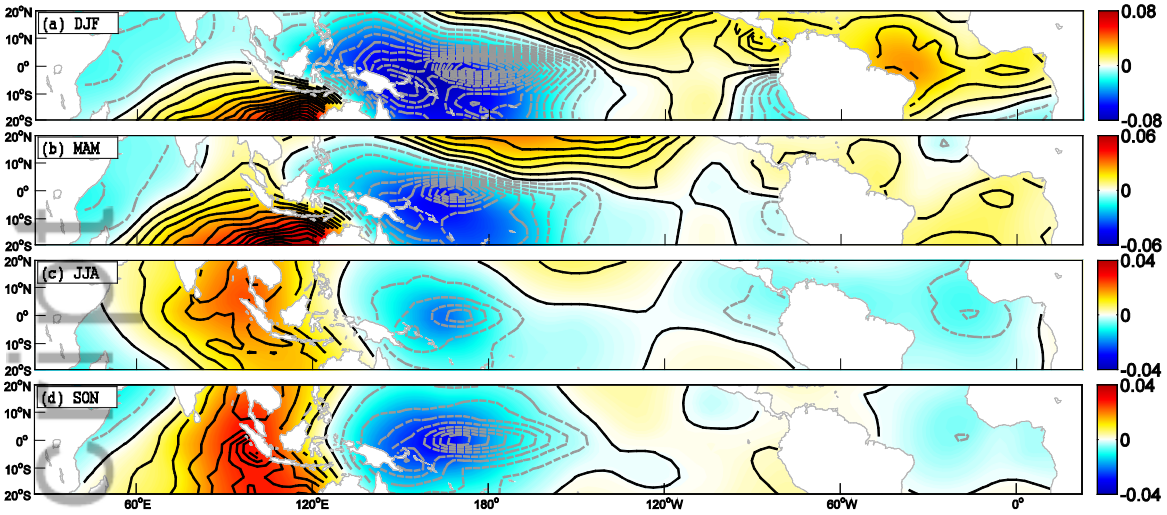

Fig. 3 Sensitivity map (shading) of precipitation over entire Australian mainland, and the product (contours) of the sensitivity and standard deviation of seasonal mean SSTs for (**a**) DJF, (**b**) MAM, (**c**) JJA, and (**d**) SON. Black solid (gray dashed) contours denote non-negative (negative) values; contour interval is 0.002 mm day^{-1}.

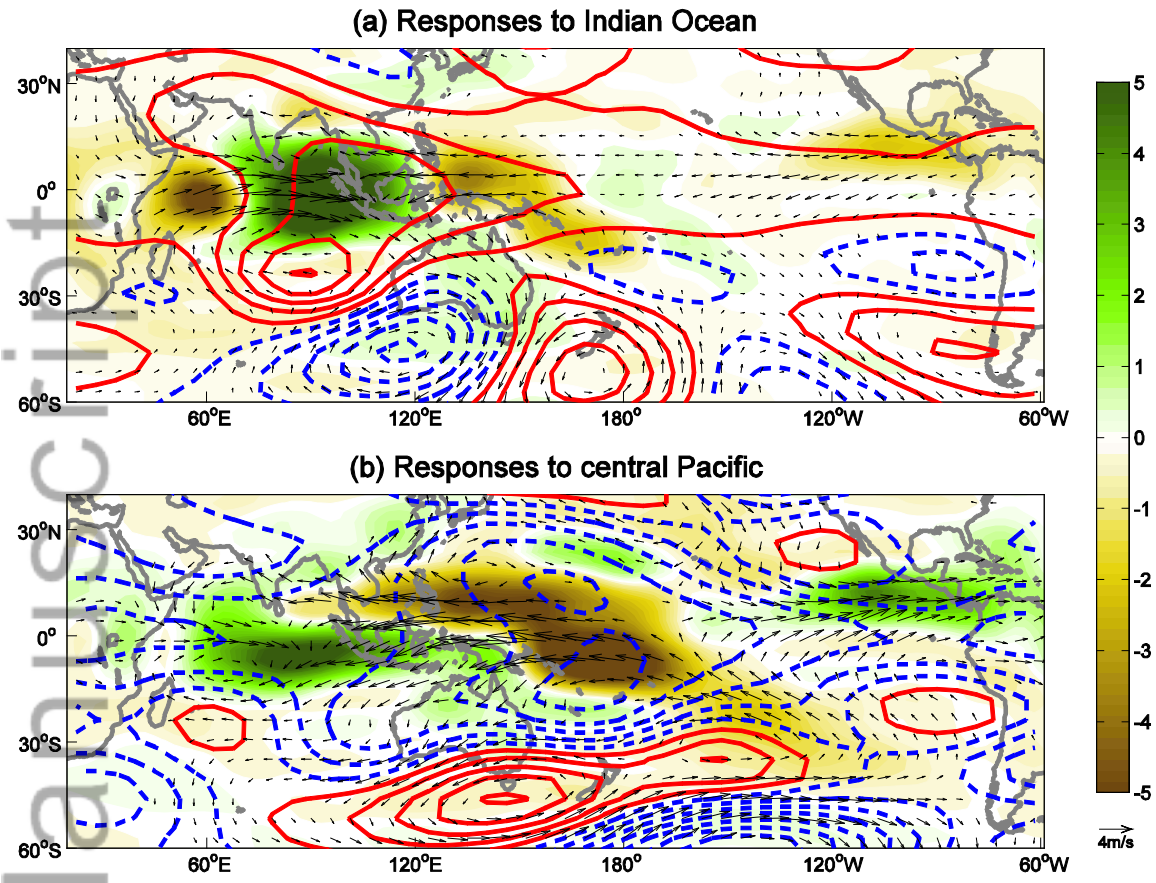

Fig. 4 Linearly constructed atmospheric responses of 200 hPa height (contours; m), precipitation (shading; mm day^{-1}), and 850-hPa winds (vectors; m s^{-1}) to hypothetical SST anomalies over (**a**) Indian Ocean (west of 130°E) and (**b**) central Pacific (140°E–140°W). The hypothetical anomalies have the same pattern as in Fig. 2b but with r.m.s. amplitude = 1 °C. Red solid (blue dashed) contours represent positive (negative) responses with an interval of 15 gpm; zero contours are omitted.

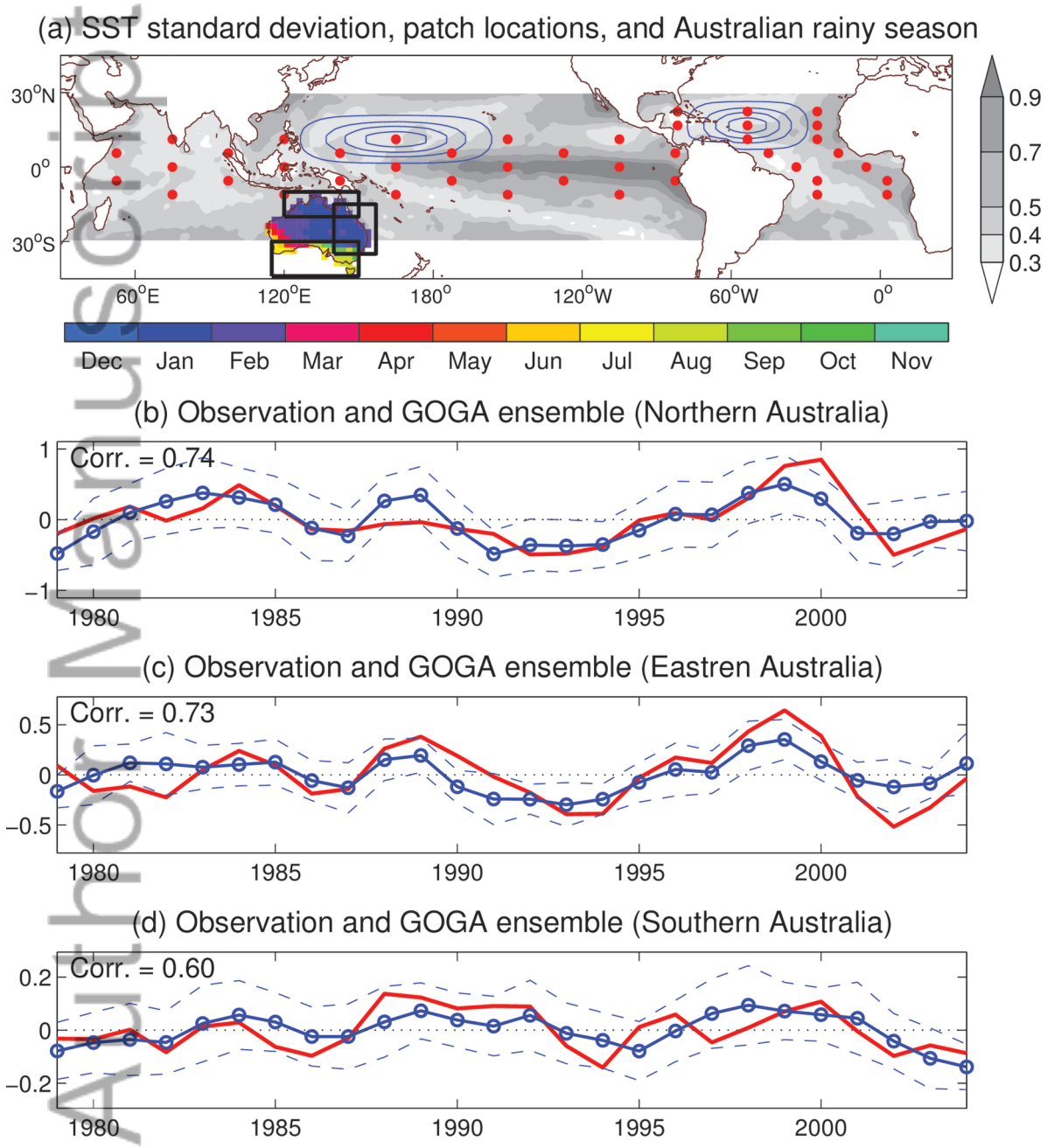

figure1

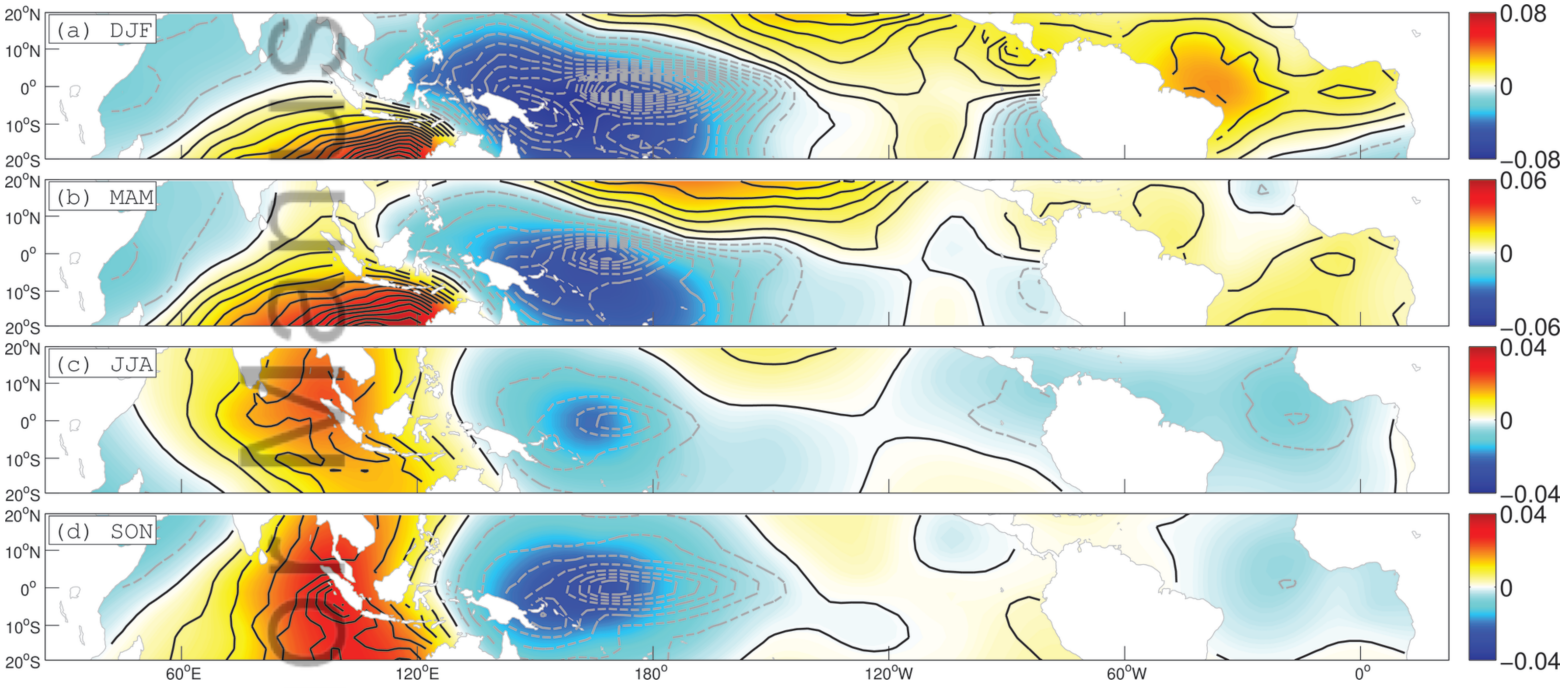

figure3

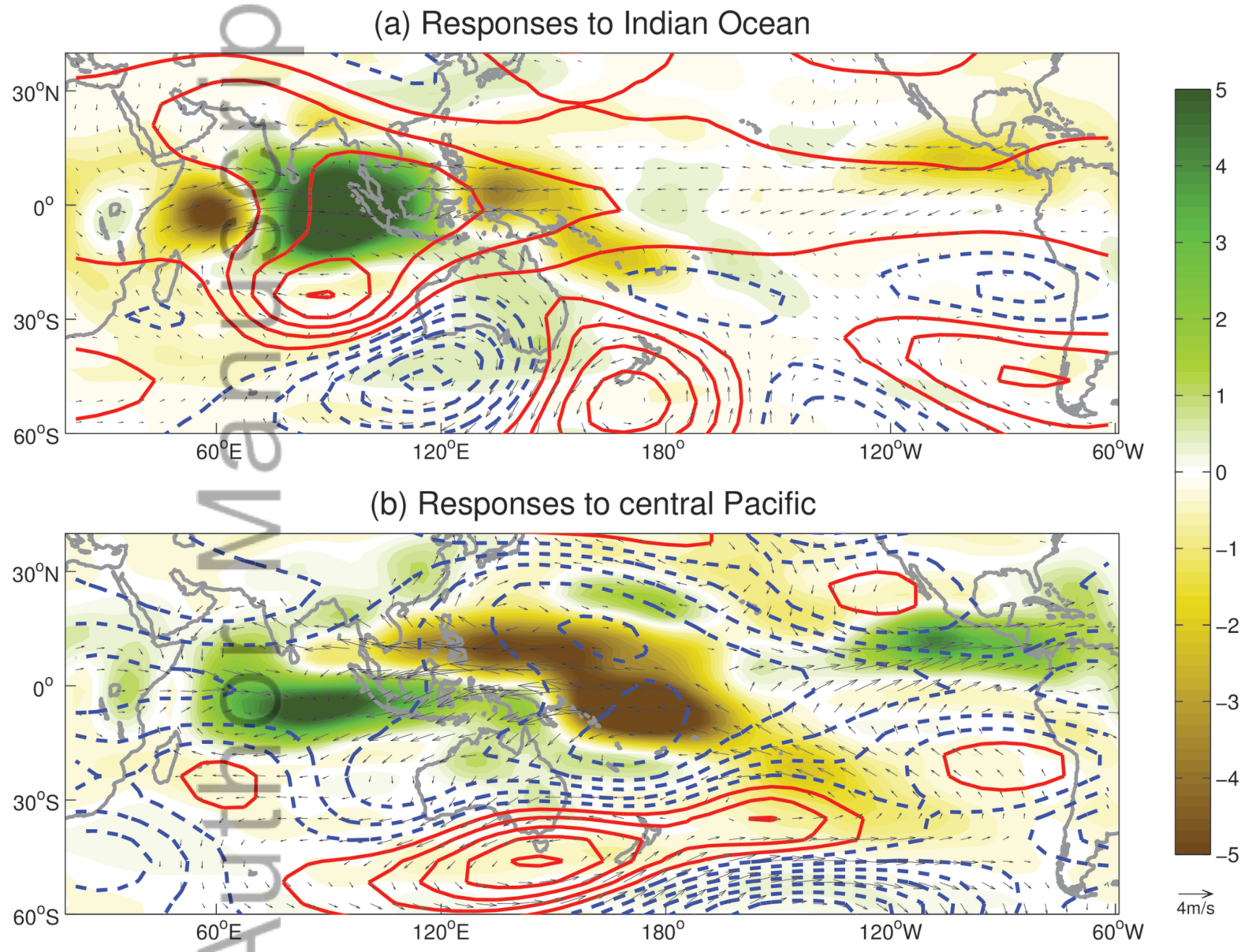

figure4

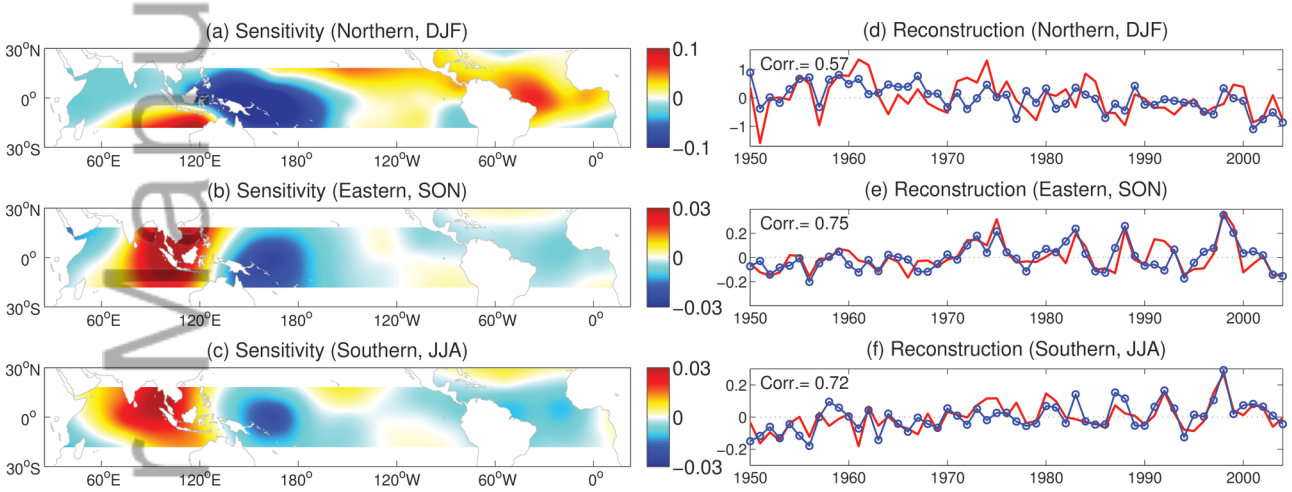

newfigure2